Theoretical Notes
Note 276

EL

DNA 3612T
-J 276

X-RAY INDUCED CURRENTS ON THE SURFACE OF A METALLIC SPHERE

Mission Research Corporation
735 State Street
Santa Barbara, California 93101

16 April 1975

Topical Report for Period August 1973—September 1974

CONTRACT No. DNA 001-74-C-0032

THIS WORK SPONSORED BY THE DEFENSE NUCLEAR AGENCY
UNDER SUBTASK R99QAXEB089-45.

Prepared for
Director
DEFENSE NUCLEAR AGENCY
Washington, D. C. 20305

UNCLASSIFIED

SECURITY CLASSIFICATION OF THIS PAGE (When Data Entered)

REPORT DOCUMENTATION PAGE		READ INSTRUCTIONS BEFORE COMPLETING FORM
1. REPORT NUMBER DNA 3612T	2. GOVT ACCESSION NO.	3. RECIPIENT'S CATALOG NUMBER
4. TITLE (and Subtitle) X-RAY INDUCED CURRENTS ON THE SURFACE OF A METALLIC SPHERE		5. TYPE OF REPORT & PERIOD COVERED Topical Report for Period August 1973—September 1974 6. PERFORMING ORG. REPORT NUMBER MRC-N-111
7. AUTHOR(s) Roger Stettner Daniel F. Higgins		8. CONTRACT OR GRANT NUMBER(s) DNA 001-74-C-0032
9. PERFORMING ORGANIZATION NAME AND ADDRESS Mission Research Corporation 735 State Street Santa Barbara, California 93101		10. PROGRAM ELEMENT, PROJECT, TASK AREA & WORK UNIT NUMBERS NWED Subtask R99QAXEB089-45
11. CONTROLLING OFFICE NAME AND ADDRESS Director Defense Nuclear Agency Washington, D.C. 20305		12. REPORT DATE 16 April 1975 13. NUMBER OF PAGES 64
14. MONITORING AGENCY NAME & ADDRESS(if different from Controlling Office)		15. SECURITY CLASS. (of this report) UNCLASSIFIED 15a. DECLASSIFICATION/DOWNGRADING SCHEDULE

16. DISTRIBUTION STATEMENT (of this Report)

Approved for public release; distribution unlimited.

17. DISTRIBUTION STATEMENT (of the abstract entered in Block 20, if different from Report)

18. SUPPLEMENTARY NOTES

This work sponsored by the Defense Nuclear Agency under Subtask R99QAXEB089-45.

19. KEY WORDS (Continue on reverse side if necessary and identify by block number)

X-ray Induced Surface Currents
Electromagnetic Ringing
Quasi-static Approximations

20. ABSTRACT (Continue on reverse side if necessary and identify by block number)

The currents on the surface of a continuous conducting sphere, caused by photo-ejection of electrons from half the surface, are found in the non-self-consistent, low fluence limit. Calculations describing the ringing of the structure, solving Maxwell's time-dependent equations, are shown to be well approximated, in certain regions, by a quasi-static approximation.

DD FORM 1 JAN 73 1473 EDITION OF 1 NOV 65 IS OBSOLETE

UNCLASSIFIED

SECURITY CLASSIFICATION OF THIS PAGE (When Data Entered)

TABLE OF CONTENTS

	PAGE
LIST OF ILLUSTRATIONS	2
SECTION 1—INTRODUCTION	3
SECTION 2—QUASI-STATIC MODEL	6
THEORY	6
CODE DESCRIPTION	11
ACCURACY	12
SECTION 3—FULLY TIME-DEPENDENT SOLUTION	15
MESH AND DIFFERENCE EQUATIONS	18
STABILITY	20
BOUNDARY CONDITIONS	25
SURFACE CURRENT AND CHARGE DENSITIES	32
TEST PROBLEM	34
DELTA FUNCTION EXCITATION	36
SECTION 4—RESULTS	41
REFERENCES	53

LIST OF ILLUSTRATIONS

FIGURE		PAGE
1	System configuration.	16
2	Radial mesh used in LFLUX.	19
3	Illustration for interpolation from retarded to real time.	33
4	Amplitude of Legendre polynomial expansion of skin currents as a function of time: Test case—spatial current density shut off at t = 1.0 shakes.	37
5	Amplitude of Legendre polynomial expansion of surface charge densities as a function of time: Test case—spatial current density shut off at t = 1.0 shakes.	38
6	Comparison of ℓ=1 skin current amplitudes. Energy range of X rays: 5 - 100 keV. Pulse duration: 3.0 shakes.	43
7	Comparison of ℓ=2 skin current amplitudes. Energy range of X rays: 5 - 100 keV. Pulse duration: 3.0 shakes.	44
8	Comparison of ℓ=3 skin current amplitudes. Energy range of X rays: 5 - 100 keV. Pulse duration: 3.0 shakes.	45
9	Comparison of ℓ=1 skin current amplitudes. Energy range of X rays: 5 = 100 keV. Pulse duration: 1.0 shakes.	46
10	Comparison of ℓ=2 skin current amplitudes. Energy range of X rays: 5 - 100 keV. Pulse duration: 1.0 shakes.	47
11	Comparison of ℓ=3 skin current amplitudes. Energy range of X rays: 5 - 100 keV. Pulse duration: 1.0 shakes.	48
12	Comparison of ℓ=1 skin current amplitudes. Energy range of X rays: 50 - 100 keV. Pulse duration: 3.0 shakes.	49
13	Comparison of ℓ=2 skin current amplitudes. Energy range of X rays: 50 - 100 keV. Pulse duration: 3.0 shakes.	50
14	Comparison of ℓ=3 skin current amplitudes. Energy range of X rays: 50 - 100 keV. Pulse duration: 3.0 shakes.	51

SECTION 1

INTRODUCTION

Recently there has been increased concern about the potential vulnerability of satellite systems to system generated electromagnetic pulse (SGEMP) effects. When a satellite is exposed to an incident X-ray pulse, photoelectrons are backscattered from the surface of the satellite, resulting in skin currents flowing on the surface and electromagnetic fields generated in the nearby space. Photons will also create electrons inside any satellite cavities and deposit charge directly on cables (IEMP effects).

In this report we will concern ourselves only with the effects of electrons ejected external to a satellite. The satellite itself will be modeled by a perfectly conducting sphere and the resulting current and charge densities on the surface of the sphere will be calculated. Such calculations are obviously idealized; real satellites are not spheres and vulnerability depends on specific circuit response rather than skin currents alone. However, our goal is to develop tools useful for SGEMP analysis rather than to carry out an actual vulnerability assessment. Thus we are trying to gain an understanding of the basic phenomena of SGEMP and such parameters as skin currents have been useful indicators of vulnerability problems for other weapon effects (e.g., EMP).

Thus the basic problem being considered is a metallic sphere being illuminated by a planar X-ray source. The X rays interact with the sphere producing backscattered electrons. (See Reference 1 for a simple model of photoelectron production.) These moving electrons form a spatial current density, which in turn creates electromagnetic fields. The

motion of the electrons is then affected by the electromagnetic fields and under some conditions many of the emitted electrons will be pulled back to the sphere from which they were emitted.

For low X-ray fluences, however, the resulting fields are small and have little effect on subsequent electron motion. Therefore, it is possible to treat the problem non-self-consistently; i.e., once electrons have been emitted they are assumed to move with a constant velocity not perturbed by the resultant fields. A method for calculating the spatial current density outside an emitting sphere is described in Reference 2. All skin current calculations described in this report are based on the low-fluence, non-self-consistent assumption.

In the following sections of the report two methods of calculating the skin currents are described. The first method assumes that the photoelectron interaction time—the time photoelectrons are effective in producing skin currents—is long compared to the periods of oscillation of the system. The fields may then be treated in accord with electrostatics. It is not necessary to calculate the fields external to the satellite with this method—only one one-dimensional integration is required—so calculations are rapid. The mathematical basis for the code, FIELD, which employs this quasi-static method is described in the next section.

Where photoelectron interaction times become comparable with the fundamental periods of oscillation of the system, the fully time dependent Maxwell equations must be used to accurately calculate the skin currents. LFLUX, a code which numerically solves the time-dependent Maxwell equations, is described in the third section.

Both computational methods employ an angular expansion in terms of Legendre polynomials. The field problem is thus set up in one spatial coordinate and time for as many polynomials as is necessary for an

accurate solution (up to six were used in our calculations). The skin currents appear as a sum of Legendre polynomials multiplied by time dependent coefficients. These coefficients are compared for two different X-ray pulse durations and two different X-ray spectra in Section 4.

SECTION 2

QUASI-STATIC MODEL

THEORY

In this section we will derive the equation used in the code FIELD. FIELD, which computes the skin currents on a metallic sphere, will then be described. We will eventually relate the skin current, as a series of Legendre polynomials, to the current of photoelectrons external to the sphere. To make this relation it is necessary to express the photoelectron current as a series in Legendre polynomials also.

As electrons are ejected from the sphere by incident X rays, the charge density, σ, on the surface of the sphere changes in time. Since charge on the surface of the sphere must satisfy the equation of continuity we can relate the surface current, K, to the time rate of change of surface charge and the current of electrons leaving normal to the surface $J_r(a)$. The equation of continuity on the surface is

$$\frac{\partial \sigma}{\partial t} = - \frac{1}{a \sin\theta} \frac{\partial}{\partial \theta}\left(K \sin\theta\right) - J_r(a) \ , \qquad (1)$$

where a is the radius of the sphere and the first term on the right-hand side of Equation 1 is the divergence of the skin current on the surface of the sphere in spherical coordinates (see Figure 1 for a definition of the coordinates). Due to the spherical symmetry of the problem, K, σ, and $J_r(a)$ can be expanded as follows:

$$K = \sum_{\ell} K_{\ell} P_{\ell}^{1}(\cos\theta) \ , \qquad (2)$$

$$\sigma = \sum_{\ell} \sigma_{\ell} P_{\ell}^{0} (\cos\theta) \ , \tag{3}$$

$$J_r = \sum_{\ell} J_{r\ell} P_{\ell}^{0} (\cos\theta) \ , \tag{4}$$

where K_ℓ and σ_ℓ are functions of time only, ℓ is an integer, P_ℓ^0 are the ordinary Legendre polynomials and P_ℓ^1 are the first associated Legendre polynomials. We will use Equation 1 to relate the coefficients of Equations 2 to those of 4. Substituting Equation 2 into Equation 1 and using the relation

$$- \frac{\partial P_{\ell}^{0}}{\partial \theta} = P_{\ell}^{1} \ , \tag{5}$$

we find

$$\frac{\partial \sigma}{\partial t} = \frac{1}{a \sin\theta} \sum_{\ell=1}^{\infty} K_{\ell} \frac{\partial}{\partial \theta} \left(\sin\theta \frac{\partial}{\partial \theta} P_{\ell}^{0} \right) - J_r \ . \tag{6}$$

Using the defining equation for Legendre polynomials

$$-\ell(\ell + 1) P_{\ell}^{0} = \frac{1}{\sin\theta} \frac{\partial}{\partial \theta} \left(\sin\theta \frac{\partial}{\partial \theta} P_{\ell}^{0} \right), \tag{7}$$

and also Equation 4 and Equation 3 in Equation 6 we obtain

$$\sum_{\ell=0}^{\infty} \left(\frac{\partial \sigma_{\ell}}{\partial t} + \frac{\ell(\ell + 1)}{a} K_{\ell} + J_{r\ell} \right) P_{\ell}^{0} = 0 \ , \tag{8}$$

or

$$K_{\ell} = - \frac{a}{\ell(\ell + 1)} \left[\frac{\partial}{\partial t} \sigma_{\ell} + J_{r\ell} \right] . \tag{9}$$

Equation 9 shows that if we can find $J_r(a)$ and σ we can expand them according to Equations 3 and 4 and obtain the coefficients of the Legendre expansion of the surface currents, essentially solving our problem.

The spatial currents are known (Reference 2) and it is a simple matter to calculate them at the surface and expand in Legendre polynomials. The surface charge is just the normal component of the electric field

multiplied by ε_0 (in MKS units), since the sphere is a perfect conductor. Therefore if we can calculate the electric field at the surface of the sphere as a function of time we can complete the solution of the problem.

Assuming we can calculate the electric field as though the system were static at any instant of time we can immediately write down the Green's function for the spherical conductor. With this Green's function, which essentially solves Poisson's equation in the space exterior to the sphere, we can find the electric field at the sphere's surface. The Green's function is

$$G(\vec{R}, \vec{R}') = \left[\frac{1}{|\vec{R} - \vec{R}'|} - \frac{a}{R' \left| \vec{R} - \frac{a^2}{R'^2} \vec{R}' \right|} - \frac{(1 - a/R')}{R} \right] \frac{1}{4\pi\varepsilon_0} \quad , \qquad (10)$$

where $\vec{R}$ is the position vector from the center of the sphere to the point exterior to the sphere at which we wish to find the field, R is the magnitude of $\vec{R}$, $\vec{R}'$ is any position vector from the center of the sphere to a point exterior to the sphere at which electrons ejected from the sphere have arrived. We denote the electron density at $\vec{R}'$ at the time t by $\rho(\vec{R}', t)$. R' is the magnitude of $\vec{R}'$.

It is found to be convenient to expand the Green's function in Legendre polynomials prior to solving for the electric field at the surface. To do so we need the relation (Reference 3)

$$\frac{1}{|\vec{R} - \vec{R}'|} = 4\pi \sum_{\ell=0}^{\infty} \sum_{m=-\ell}^{\ell} \frac{1}{2\ell + 1} \frac{R_<^{\ell}}{R_>^{\ell + 1}} Y_{\ell m}^*(\theta', \phi') \, Y_{\ell m}(\theta, \phi) \quad , \qquad (11)$$

where $R_>$ and $R_<$ refer to the larger or smaller of R and R'; $Y_{\ell m}$ are spherical harmonics and θ, ϕ are the angular spherical coordinates of the point at $\vec{R}$. A similar expansion can be made for the second term on the right-hand side of Equation 10. Primes refer to the point $\vec{R}'$. Expanding Equation 10 with the aid of Equation 11 while noting that the surface charge $\sigma(t, \theta)$ is given by the expression

$$\sigma(t,\theta) = E_r(a,\ \theta,\ t)\ \varepsilon_0\ , \tag{12}$$

where

$$E_r(a,\ \theta,\ t) = -\frac{\partial}{\partial R}\Phi\ \Big|_{r=a}\ , \tag{13}$$

and also noting

$$\Phi(\vec{R},\ t) = \int \rho(\vec{R}',\ t)G(\vec{R}',\ R)d\vec{R}'\ , \tag{14}$$

(where again $\rho(\vec{R}',\ t)$ is the spatial charge density of electrons external to the sphere) we find , after integrating over ϕ', that

$$\sigma(t,\ \theta) = \frac{1}{2}\sum_{\ell=1}^{\infty} a^{\ell-1}\,(2\ell+1)P_\ell^0(\cos\theta)\iint P_\ell^0(\cos\theta')\ \frac{\rho(\vec{R}',\ t)}{R'^{(\ell+1)}}\ R'^2 dR'd\cos\theta'$$

$$+\ \frac{1}{2}\frac{1}{a^2}\iint \rho(\vec{R}',\ t)R'^2 dR'd\cos'\ . \tag{15}$$

Taking the time derivative of Equation 15 we can relate the time rate of change of the charge density on the sphere to the time rate of change of spatial charge density. We find

$$\frac{\partial\sigma(t,\ \theta)}{\partial t} = \frac{1}{2}\sum_{\ell=1}^{\infty} a^{\ell-1}\,(2\ell+1)P_\ell^0(\cos\theta)\iint P_\ell^0(\cos\theta')\frac{\partial\rho}{\partial t}\,R'^{-(\ell-1)}dR'd\cos\theta'$$

$$+\ \frac{1}{2}\frac{1}{a^2}\iint \frac{\partial\rho}{\partial t}\,R'^2 dR'd\cos'\ . \tag{16}$$

We can relate $\frac{\partial\rho}{\partial t}$ to the spatial current densities by the equation of continuity. If $J_r(\vec{R}',\ t)$ and $J_\theta(\vec{R}',\ t)$ denote the radial and angular components of the spatial current density the equation of continuity takes the form

$$-\frac{\partial\rho}{\partial t} = \frac{1}{R'^2}\frac{\partial}{\partial R'}\,(R'^2 J_r) + \frac{1}{R'\sin\theta'}\frac{\partial}{\partial\theta'}\,(\sin\theta' J_\theta)\ . \tag{17}$$

Substituting Equation 17 into Equation 16 and integrating by parts, while noting $J_r(\infty,t)$ is zero and J_θ is also zero at $\theta = 0$ and $\theta = \pi$, we have

$$\frac{\partial\sigma(t,\ \theta,\ a)}{\partial t} = \sum_{\ell=1}^{\infty} a^{\ell-1}\ \frac{(2\ell+1)}{2}\ P_\ell^0(\cos\theta)\iint (J_r P_\ell^0 + J_\theta P_\ell^1)R'^{-\ell}dR'd\cos\theta'$$

$$- \sum_{\ell=1}^{\infty}\left(\frac{2\ell+1}{2}\right)P_\ell(\cos\theta)\int_1^{-1} J_r(a,\ \theta',\ t)P_\ell^0(\cos\theta')d\cos\theta'$$

$$- \frac{1}{2}\int_1^{-1} J_r(a,\ \theta',\ t)d\cos\theta' \ . \qquad (18)$$

If we expand the spatial currents in Legendre polynomials we can find the $\partial\sigma_\ell/\partial t$ terms in Equation 9 in terms of integrals of the Legendre coefficients of J_r and J_θ over the range of the spatial variable R'. If the expansions of J_r on J_θ are

$$J_r(\theta',\ R',\ t) = \sum_{\ell=0}^{\infty} J_{r_\ell}(R',\ t)P_\ell^0(\cos\theta') \ , \qquad (19)$$

and

$$J_\theta(\theta',\ R',\ t) = \sum_{\ell=1}^{\infty} J_{\theta_\ell}(R',\ t)P_\ell^1(\cos\theta') \ , \qquad (20)$$

then we find by substitution in Equation 18 that

$$\frac{\partial\sigma}{\partial t}\ (t,\ \theta,\ a) = \sum_{\ell=1}^{\infty} P_\ell^0 a^{\ell-1}\int \frac{(\ell+1)(J_{r_\ell} + \ell J_{\theta_\ell})dR'}{R'^{\ell}}$$

$$- \sum_{\ell=0}^{\infty} P_\ell^0 J_{r_\ell}(a,\ t) \ , \qquad (21)$$

comparing Equation 21 with the time derivative of Equation 3 we find

$$\frac{\partial\sigma_0}{\partial t} = - J_{r_0}(a,\ t) \ , \qquad (22)$$

and

$$\frac{\partial \sigma_\ell}{\partial t} = a^{\ell-1}(\ell + 1)\int_a^\infty (J_{r_\ell} + \ell J_{\theta_\ell})R'^{-\ell} dR' - J_{r_\ell}(a, t) \ . \qquad (23)$$

$$\ell \geq 1$$

Noting that $J_{r_\ell}(a, t)$ is just equal to J_{r_ℓ} in Equation 4 we can substitute Equation 23 into 9 to obtain the Legendre coefficients of the skin current:

$$K_\ell(t) = -\frac{a^\ell}{\ell}\int_a^\infty (J_{r_\ell}(R', t) + \ell J_{\theta_\ell}(R', t))R'^{-\ell} dR' \ . \qquad (24)$$

Equation 24 is the simple relation referred to in the first paragraph of this section.

CODE DESCRIPTION

We now discuss the coding of FIELD which solves Equation 24 for the Legendre coefficients of the skin currents. The spatial currents J_r and J_θ are obtained from an approximation or another code (Reference 2). These currents are then expanded in Legendre polynomials. The Legendre coefficients $J_{r\ell}(R', t)$ and $J_{\theta\ell}(R', t)$ are found for various values of R' and t, in the significant ranges of those variables, and the numbers stored on tape in the form of a table. When a particular value of $J_{r\ell}(R', t)$ is needed for the integrand of Equation 24, for example, a linear interpolation is made between J_{r_ℓ} values in the table. Because of the rapid convergence of the polynomial series for skin currents the maximum ℓ in the table is five.

It is necessary to evaluate the integral in Equation 24 only where the integrand is non-zero so that the limits of integration are not really from a to ∞. Electrons emitted from the sphere travel at a finite velocity so the integrand will be zero beyond the point where the fastest electrons have arrived which were first emitted from the sphere. If we denote the

largest speed by VL and the time counted from when the X ray first strikes the sphere, by t, the upper limit on the integration is a + VL multiplied by t. The X-ray pulse lasts only for a time τ after which the integrand is zero in the R' range between the surface of the sphere and the slowest electron. Denote the speed of the slowest electron by VS. The lower limit of integration in Equation 24 is a for $t < \tau$ and a + VS multiplied by t for $t > \tau$. In actual computation it turns out that the effective VS is actually somewhat greater than the slowest electron speed and the actual VL is smaller than the greatest electron speed.

At each time t the range of integration is broken up into fifty spatial intervals. At this t the table is called for the fifty one R' values and the numerical integration of Equation 24 is obtained using Simpson's rule (Reference 4). For the problems considered τ was at most 5×10^{-8} sec and the interval between time steps was 1.0×10^{-10} sec.

FIELD is designed specifically for a sphere and for a non-self-consistent approximation. The running time for a typical problem is 3.6 sec on a CDC 7600.

ACCURACY

One can get a quantitative idea of the correction the time-dependent Maxwell equation solution makes upon the quasi-static solution by looking at the equation for the scalar potential in the Lorentz gauge (Reference 3). This equation is

$$\nabla^2\Phi - \frac{1}{c^2}\frac{\partial^2\Phi}{\partial t^2} = -4\pi\rho \ , \qquad (25)$$

where as before Φ is the scalar potential and ρ is the spatial charge density. If we look for an asymptotic solution of Equation 25 which has the form

$$\Phi = \Phi_0 + \alpha\Phi_1 + \alpha^2\Phi_2 + \ldots \ , \qquad (26)$$

where Φ_0 is the quasi-static solution and Φ_1 is the first correction to it, we find that

$$\Phi_1/\Phi_0 \sim \left(\frac{\lambda}{cT'}\right)^2 \equiv \alpha \ , \tag{27}$$

where λ is the wavelength of the system and T' is the effective period of the interaction. In the problems considered in this report T' is equal to the duration of the X-ray pulse, T, plus the pulse lengthening due to electron flight time, plus the time it takes light (the X rays) to cross the system. For the electron spectra considered in this report the upper limit on effective flight time lengthening is somewhat less than 2×10^{-8} sec (Reference 2). The parameter α is calculated in Table 1 for the wavelengths corresponding to the first three modes of oscillation of the sphere for X-ray pulse lengths of 3×10^{-8} sec and 1×10^{8} sec. For example with a pulse length of 3×10^{-8} sec, one would expect the quasi-static approach to be, in some sense, no more than about 23% in error. With a pulse length of 1×10^{-8} sec, this error should increase to about 64%. As will be explained in Section 4, Table 1 compares favorably with the code results.

TABLE I

MODE	WAVELENGTH	DURATION OF PULSE, T	$\left(\frac{\lambda}{c(T+2\times10^{-8})}\right)^2$
1	7.3a	3×10^{-8} sec	.23
2	3.5a	3×10^{-8} sec	.05
3	2.3a	3×10^{-8} sec	.02
1	7.3a	1×10^{-8} sec	.64
2	3.5a	1×10^{-8} sec	.15
3	2.3a	1×10^{-8} sec	.06

SECTION 3

FULLY TIME-DEPENDENT SOLUTION

INTRODUCTION

In the previous section, a quasi-static method for solving SGEMP skin currents was discussed. In this section, we will derive a method for finding the fully time-dependent solution using a finite difference solution of Maxwell's equations.

The code used for solving Maxwell's equations is called LFLUX. Again, we assume electrons are emitted from a perfectly conducting sphere (see Figure 1) and azimuthal symmetry is required. Spatial current densities are assumed known (see Reference 2) and thus electron motion is not treated self-consistently.

We will first develop the basic theory used, including such factors as difference equations, stability criteria, and boundary conditions. Then, the results will be compared with theoretical calculations for a simple test problem.

MAXWELL'S EQUATIONS

In MKS units, Maxwell's two curl equations are

$$\frac{1}{\mu} \nabla \times \vec{B} = \vec{J} + \sigma \vec{E} + \varepsilon \frac{\partial \vec{E}}{\partial t} , \tag{28}$$

$$\nabla \times \vec{E} = - \frac{\partial \vec{B}}{\partial t} . \tag{29}$$

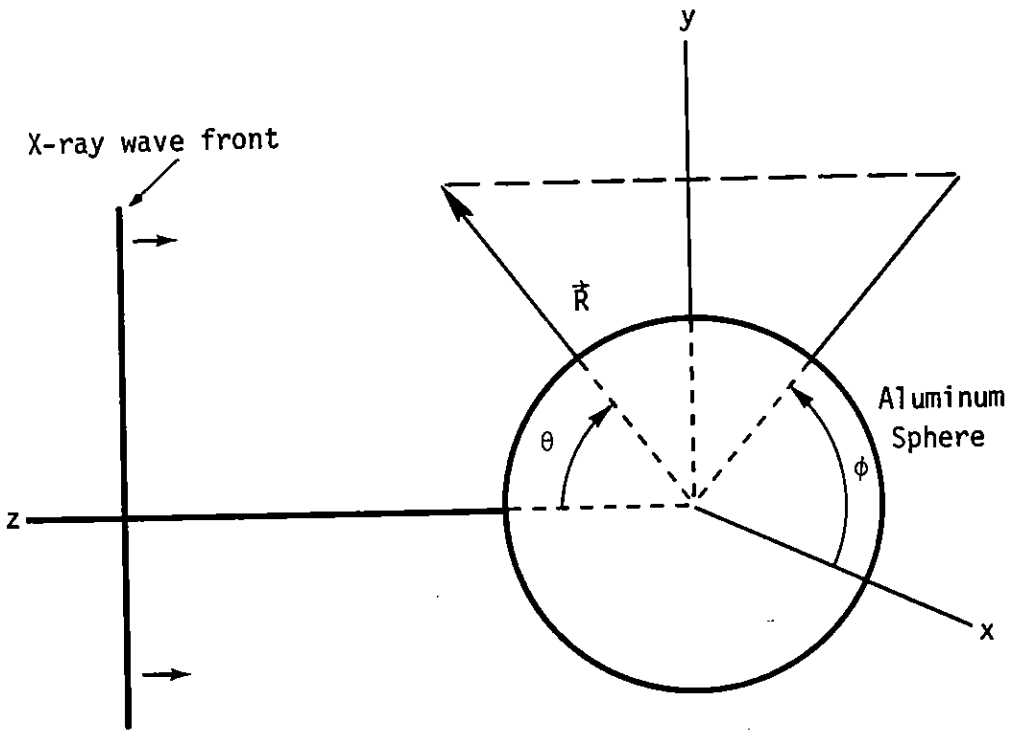

Figure 1. System configuration.

We now write these equations in spherical coordinates with the assumption of azimuthal symmetry. (For a more complete derivation, see Reference 5.) The two above vector equations then become

$$\frac{1}{\mu r \sin\theta} \frac{\partial}{\partial \theta} [B'_\phi \sin\theta] = J_r + \sigma E_r + \varepsilon \frac{\partial E_r}{\partial t} , \tag{30}$$

$$- \frac{1}{\mu r} \frac{\partial}{\partial r} [r B'_\phi] = J_\theta + \sigma E'_\theta + \varepsilon \frac{\partial E'_\theta}{\partial t} , \tag{31}$$

and

$$\frac{1}{r} \left[\frac{\partial}{\partial r} (r E'_\theta) - \frac{\partial E_r}{\partial \theta} \right] = - \frac{\partial B'_\phi}{\partial t} . \tag{32}$$

We can now remove the θ-dependence by expanding in terms of Legendre polynomials; i.e., we write

$$\left.\begin{aligned} J_r &= \sum_\ell J_{r_\ell} P_\ell^0(\cos\theta) \\ J_\theta &= \sum_\ell J_{\theta_\ell} P_\ell^1(\cos\theta) \\ E_r &= \sum_\ell E_{r_\ell} P_\ell^0(\cos\theta) \\ E'_\theta &= \sum_\ell E'_{\theta_\ell} P_\ell^1(\cos\theta) \\ B'_\phi &= \sum_\ell B'_{\phi_\ell} P_\ell^1(\cos\theta) \end{aligned}\right\} \tag{33}$$

where $P_\ell^0(\cos\theta)$ is the ordinary Legendre polynomial and $P_\ell^1(\cos\theta)$ is the first associated Legendre polynomial.

Equation 30, 31, and 32 then become

$$\frac{\ell(\ell + 1)}{\mu r} B'_{\phi_\ell} = J_{r_\ell} + \varepsilon \frac{\partial}{\partial t} E_{r_\ell} , \tag{34}$$

$$-\frac{1}{\mu r}\frac{\partial}{\partial r}\left[rB'_{\phi_\ell}\right] = J_{\theta_\ell} + \varepsilon\frac{\partial E'_{\theta_\ell}}{\partial t}\,, \tag{35}$$

$$\frac{1}{r}\left[\frac{\partial}{\partial r}\left(rE'_{\theta_\ell}\right) + E_{r_\ell}\right] = -\frac{\partial}{\partial t}B'_{\phi_\ell}\,, \tag{36}$$

where we have also assumed that all charge is included in the $\vec{J}$ term so that the conductivity, σ, is zero.

For simplicity, we will now drop the ℓ subscripts and we will make the substitutions

$$B_\phi = rB'_\phi\,, \tag{37}$$

$$E_\theta = rE'_\theta\,, \tag{38}$$

Equations 34, 35, and 36 then reduce to

$$\frac{\partial B_\phi}{\partial t} = -E_r - \frac{\partial}{\partial r}E_\theta\,, \tag{39}$$

$$\frac{\partial E_r}{\partial t} = -\frac{J_r}{\varepsilon} + \frac{\ell(\ell+1)}{\varepsilon\mu r^2}B_\phi\,, \tag{40}$$

$$\frac{\partial E_\theta}{\partial t} = -\frac{r}{\varepsilon}J_\theta - \frac{1}{\varepsilon\mu}\frac{\partial}{\partial r}B_\phi\,, \tag{41}$$

MESH AND DIFFERENCE EQUATIONS

As a result of expanding the variables in Maxwell's equations in terms of Legendre polynomials, we need to difference Equations 39, 40, and 41 in terms of time and radial distance r only. Let us consider an evenly spaced radial mesh. If we examine Equation 39 and center the difference equation, it is easily seen that we require B_ϕ and E_r values at one mesh point and E_θ values at adjacent mesh points. This is consistent with the other two differential equations and the resulting mesh is indicated in Figure 2.

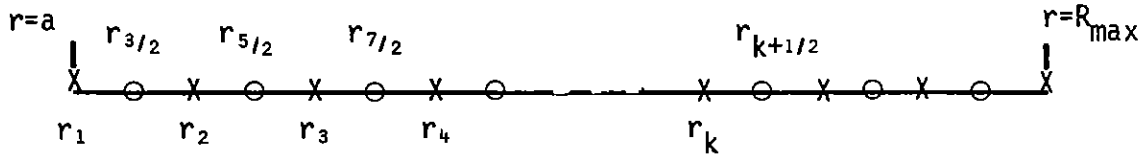

X indicates points where E_θ is calculated

O indicates points where B_ϕ, E_r are calculated

Figure 2. Radial mesh used in LFLUX.

Let us assume that points in the time mesh are also equally spaced with time step δt and let n refer to time grid points and k to spacial grid points. Then if we center Equation 39 at n and k + 1/2, the resulting difference equation is

$$B_{\phi_{k+1/2}}^{n+1/2} = B_{k+1/2}^{n-1/2} + \delta t \left[- E_{r_{k+1/2}}^{n} - \frac{E_{\theta_{k+1}}^{n} - E_{\theta_k}^{n}}{r_{k+1} - r_k} \right] . \qquad (42)$$

Centering Equation 40 at n+1/2 and k+1/2, one obtains

$$E_{r_{k+1/2}}^{n+1} = E_{r_{k+1/2}}^{n} + \delta t \left[- \frac{1}{\varepsilon} J_{r_{k+1/2}}^{n+1/2} + \frac{\ell(\ell+1)}{\varepsilon\mu r_{k+1/2}^2} B_{\phi_{k+1/2}}^{n+1/2} \right] . \qquad (43)$$

Likewise, one centers 41 at n+1/2 and k, with the result

$$E_{\theta_k}^{n+1} = E_{\theta_k}^{n} + \delta t \left[- \frac{r_k}{\varepsilon} J_{\theta_k}^{n+1/2} - \frac{1}{\varepsilon\mu} \frac{\left(B_{\phi_{k+1/2}}^{n+1/2} - B_{k-1/2}^{n+1/2} \right)}{\left(r_{k+1/2} - r_{k-1/2} \right)} \right] . \qquad (44)$$

Thus Equations 42, 43, and 44 are the three difference equations used in the LFLUX code.

STABILITY

One important question regarding any set of difference equations is that of stability. One method of checking stability is to assume a small perturbation and then see if this perturbation grows with time. For example, assume

$$\left.\begin{aligned} B_\phi &\to B_\phi + \delta B_\phi \\ E_\theta &\to E_\theta + \delta E_\theta \\ \text{and} \qquad E_r &\to E_r + \delta E_r \end{aligned}\right\}, \tag{45}$$

where δB_ϕ, δE_θ, and δE_r are all small changes in the fields. These new perturbed fields must also satisfy Maxwell's equations and if these new fields are substituted into Equations 42, 43, and 44 we have the result that the perturbations must be solutions of homogeneous forms of Equations 42, 43, and 44; i.e.,

$$\delta B_{\phi_{k+1/2}}^{n+1/2} = \delta B_{\phi_{k+1/2}}^{n-1/2} + \delta t\left[-\delta E_{r_{k+1/2}}^{n} - \frac{E_{\theta_{k+1}}^{n} - E_{\theta_k}^{n}}{r_{k+1} - r_k}\right], \tag{46}$$

$$\delta E_{r_{k+1/2}}^{n+1} = \delta E_{r_{k+1/2}}^{n} + \delta t\left[\frac{\ell(\ell+1)}{\epsilon\mu}\,\delta B_{\phi_{k+1/2}}^{n+1/2}\right], \tag{47}$$

and

$$\delta E_{\theta_k}^{n+1} = \delta E_{\theta_k}^{n} + \delta t\left[-\frac{1}{\epsilon\mu}\,\frac{\left(\delta B_{\phi_{k+1/2}}^{n+1/2} - \delta B_{\phi_{k-1/2}}^{n+1/2}\right)}{\left(r_{k+1/2} - r_{k-1/2}\right)}\right]. \tag{48}$$

Let us refer to any of the three field perturbations as $\delta f(r, t)$. We then assume that the perturbation can be written

$$\delta f(r, t) = f_0 e^{\alpha t - ikr} \quad . \tag{49}$$

This expression is just one Fourier component of the Fourier expansion of the perturbation. Now let

$$\chi = e^{\alpha \delta t} \quad , \tag{50}$$

and

$$\phi = k\delta r \quad . \tag{51}$$

Using a perturbation of the form of Equation 49 in Equations 46, 47 and 48, one obtains a determinant relating the coefficients, namely

$$\begin{vmatrix} \sqrt{\chi} - \frac{1}{\sqrt{\chi}} & \delta t & \delta t \left[\frac{e^{i\phi/2} - e^{-i\phi/2}}{\delta r} \right] \\ - \frac{\ell(\ell+1)}{\varepsilon\mu r^2} \delta t \sqrt{\chi} & \chi - 1 & 0 \\ \frac{1}{\varepsilon\mu} \frac{\delta t}{\delta r} \sqrt{\chi} \left(1 - e^{-i\phi}\right) & 0 & (\chi - 1)\, e^{-i\phi/2} \end{vmatrix} = 0 \tag{52}$$

By multiplying the first column by $\sqrt{\chi}$ and the third row by $e^{i\phi/2}$ and making the substitution

$$\sin \frac{\phi}{2} = \frac{1}{2i} \left[e^{i\phi/2} - e^{-i\phi/2} \right] \tag{53}$$

the determinant equation becomes

$$\begin{vmatrix} \chi - 1 & \delta t & 2i \frac{\delta t}{\delta r} \sin \frac{\phi}{2} \\ - \frac{\ell(\ell + 1)}{\epsilon\mu r^2} \delta t \chi & \chi - 1 & 0 \\ \frac{1}{\epsilon\mu} \frac{\delta t}{\delta r} \chi \left(2i \sin \frac{\phi}{2}\right) & 0 & \chi - 1 \end{vmatrix} = 0 \qquad (54)$$

which reduces to

$$(\chi - 1)^3 + (\chi - 1) \frac{\chi \delta t^2 \ell(\ell + 1)}{\epsilon\mu r^2} + \frac{4}{\epsilon\mu} (\chi - 1) \chi \left(\frac{\delta t}{\delta r}\right)^2 \sin^2 \frac{\phi}{2} = 0 \qquad (55)$$

Since we can factor out a $(\chi - 1)$ term, $\chi = 1$ is one solution of this cubic equation. After factoring out this $(\chi - 1)$ term, the equation becomes quadratic and can be solved for χ by the quadratic formula with the result that

$$\chi = \frac{- \beta \pm \sqrt{\beta^2 - 4}}{2} \qquad (56)$$

where

$$\beta = - 2 + \frac{\ell(\ell + 1)}{\epsilon\mu} \frac{\delta t^2}{r^2} + \frac{4}{\epsilon\mu} \left(\frac{\delta t}{\delta r}\right)^2 \sin^2 \frac{\phi}{2} \qquad (57)$$

For stability, we require that the perturbations do not grow exponentially with time. This is equivalent to requiring that

$$|\chi|^2 \leq 1 \text{ for all } \phi \qquad (58)$$

Let us first assume that the term under the radical in Equation 56 is greater than or equal to zero. Then

$$|\chi|^2 = \chi^2 = \tfrac{1}{2}\beta^2 \mp \beta\sqrt{\beta^2 - 4} - 1 \tag{59}$$

and the stability requirement becomes

$$\beta^2 - 4 \leq \pm \beta\sqrt{\beta^2 - 4} \tag{60}$$

Since we originally assumed that $\beta^2 - 4 \geq 0$, the minus sign solution is immediately ruled out for positive β; similarly, the positive sign is ruled out for negative β. Thus there is no region where both solutions for χ satisfy the stability requirement (equation 58) and $\beta^2 - 4 \geq 0$. We must therefore investigate the case where $\beta^2 - 4 \leq 0$.

$$\text{For } \beta^2 - 4 \leq 0, \ \chi \text{ has an imaginary part and } |\chi|^2 = \chi\chi^* \tag{61}$$

where * indicates taking the complex conjugate. Then

$$|\chi|^2 = \frac{\left(-\beta + i\sqrt{|\beta^2 - 4|}\right)\left(-\beta - i\sqrt{|\beta^2 - 4|}\right)}{4} = 1 \tag{62}$$

Thus we have shown that our difference equations are stable provided that

$$\beta^2 - 4 \leq 0 \tag{63}$$

Going back to the definition of β (equation 57), this is equivalent to

$$\ell(\ell + 1)\left[\frac{c\delta t}{r}\right]^2 + 4\left[\frac{c\delta t}{\delta r}\right]^2 \sin^2\phi \leq 4 \tag{64}$$

where we have assumed the medium surrounding the sphere is free space so that

$$\varepsilon = \varepsilon_0 \tag{65}$$

$$\mu = \mu_0 \tag{66}$$

and

$$c^2 = \frac{1}{\varepsilon_0 \mu_0} \tag{67}$$

where c is the velocity of light in a vacuum.

Since stability requires that the inequality in (64) holds for all values of ϕ, we can replace sin ϕ by its maximum value, 1, with the result that

$$(c\delta t)^2 \frac{\ell(\ell + 1)}{r^2} + 4 \left(\frac{c\delta t}{\delta r}\right)^2 \leq 4 \tag{68}$$

Thus the Currant condition, $c\delta t \leq \delta r$, is a necessary but not sufficient condition for stability. Stability also depends on the order of the Legendre polynomial being used (the value of ℓ) and the distance from the origin, r. This dependence is quite reasonable when one considers that the Legendre polynomial expansion must be equivalent to meshing Maxwell's equations in both r and θ. With such a two-dimensional mesh, stability should depend on both the radial and angular mesh sizes.

In the LFLUX code, the radial mesh size, δr, is an input parameter. The size of the time step, δt, is then determined by re-writing equation 68 as

$$(c\delta t)^2 = f_s \left[\frac{1}{\frac{\ell(\ell + 1)}{4r^2} + \frac{1}{(\delta r)^2}}\right] \tag{69}$$

where the fractional stability, f_s, (also an input parameter) is required to be less than or equal to one. By setting r equal to a, the inner radius of the mesh, and ℓ equal to the maximum order Legendre polynomial being considered, Equation 69 gives the size of time step required for stability.

BOUNDARY CONDITIONS

From the mesh shown in Figure 2 it is apparent that as boundary conditions we must know the value of E_θ at the inner and outer values of the radial mesh at all times in order to determine the other field values.

Inner Boundary Condition

We assume that the inner sphere (which emits electrons) is a perfect conductor. Therefore, at the inner boundary of the radial grid (i.e., at the surface of the sphere) E_θ is just zero at all times.

Outer Boundary Condition

We also need to know E_θ at some outer boundary which is at a distance R_{max}. One useful outer boundary condition is to assume that a perfect conductor also exists at $r = R_{max}$. Then, as with the inner boundary, we just have the requirement that E_θ is zero at the boundary at all times. Such a conducting outer boundary is useful for modeling such things as the SGEMP response of a satellite inside a large vacuum tank being used for simulation purposes. Such an outer boundary condition is somewhat unrealistic, however, for modeling the free space SGEMP response of a structure because the inner sphere is electromagnetically coupled to the outer conductor. The conductors are isolated by transit time effects, though, and if R_{max} is large compared to the radius of the inner sphere the early time waveforms will be identical to those in free space (i.e., no outer conductor). Moving the outer boundary to large distances requires a large number of radial mesh points and thus increases both storage requirements and running time.

A second method for treating the outer boundary condition is to pick an outer boundary beyond which the source currents are zero and require that only outgoing electromagnetic waves exist at this boundary. A similar

technique has been used in the LEMP code (references 6,7) and the discussion here is based on an improvement of that method*.

We assume that the radial mesh ends at $r = R_{max}$ where R_{max} is an input parameter chosen so that no source currents exist for $r > R_{max}$ for times of interest. Then for $r > R_{max}$, Maxwell's equations become (after being expanded in terms of Legendre polynomials - see equations 39, 40, 41)

$$\frac{\partial B_\phi}{\partial t} = - E_r - \frac{\partial E_\theta}{\partial r} \tag{70}$$

$$\frac{\partial E_r}{\partial t} = \frac{\ell(\ell + 1)}{\epsilon_0 \mu_0} B_\phi \tag{71}$$

and

$$\frac{\partial E_\theta}{\partial t} = - \frac{1}{\epsilon_0 \mu_0} \frac{\partial B_\phi}{\partial r} \tag{72}$$

We now make the transformations

$$F \equiv E_\theta + cB_\phi \tag{73}$$

$$G \equiv E_\theta - cB_\phi \tag{74}$$

$$\tau \equiv ct - r \tag{75}$$

$$r' \equiv r \qquad \text{(prime dropped after transformation)}$$

*Developed by J. Longley of MRC.

After this transformation, equations 70, 71, and 72 become

$$\frac{\partial E_r}{\partial \tau} = \frac{\ell(\ell + 1)}{2r^2} (F - G) \tag{76}$$

$$\frac{\partial F}{\partial r} = - E_r \tag{77}$$

$$2 \frac{\partial G}{\partial \tau} - \frac{\partial G}{\partial r} = E_r \tag{78}$$

where each field component is actually the ℓ^{th} part of a Legendre polynomial expansion and the differential equations are now in terms of retarded time.

Now let us expand each of the field components in reciprocal powers of r; i.e., let

$$E_r (r,\tau) = e_0(\tau) + \frac{e_1(\tau)}{r} + \frac{e_2(\tau)}{r^2} + \ldots \tag{79}$$

$$F (r,\tau) = f_0(\tau) + \frac{f_1(\tau)}{r} + \frac{f_2(\tau)}{r^2} + \ldots \tag{80}$$

$$G (r,\tau) = g_0(\tau) + \frac{g_1(\tau)}{r} + \frac{g_2(\tau)}{r^2} + \ldots \tag{81}$$

One can now take these series expansions plug them into Equations 76, 77 and 78, and then equate coefficients of equal powers of r. Equation 76 then gives

$$\begin{aligned} e_0' &= 0 \\ e_1' &= 0 \\ e_2' &= \frac{\ell(\ell + 1)}{2} \left(f_0 - g_0\right) \\ e_3' &= \frac{\ell(\ell + 1)}{2} \left(f_1 - g_1\right) \\ &\vdots \\ e_i' &= \frac{\ell(\ell + 1)}{2} \left(f_{i-2} - g_{i-2}\right) \end{aligned} \tag{82}$$

while Equation 77 results in

$$
\begin{aligned}
e_0 &= 0 \\
e_1 &= 0 \\
f_1 &= e_2 \\
f_2 &= \tfrac{1}{2} e_3 \\
&\vdots \\
f_i &= \frac{1}{i} e_{i+1}
\end{aligned}
\tag{83}
$$

and equation 78 gives

$$
\begin{aligned}
g_0' &= \tfrac{1}{2} e_0 \\
g_1' &= \tfrac{1}{2} e_1 \\
g_2' &= \tfrac{1}{2} \left(-g_1 + e_2 \right) \\
&\vdots \\
g_i' &= \tfrac{1}{2} \left[-(i-1)\, g_{i-1} + e_i \right]
\end{aligned}
\tag{84}
$$

where $' \equiv \frac{\partial}{\partial \tau}$ and the subscript i refers to the coefficient of the r^{-i} term in the series expansion.

If we combine these results, one obtains

$$
g_i' = \frac{i(i-1)}{\ell(\ell+1)} f_i' \tag{85}
$$

Integrating this equation with respect to retarded time gives

$$
g_i = \frac{i(i-1)}{\ell(\ell+1)} f_i + \text{constant.} \tag{86}
$$

The assumption that we have only outgoing waves is identical to the requirement that the fields are zero at $\tau = -\infty$. Thus, the constant in equation 86 is zero.

Similarly, one can show that

$$
e_i = \frac{\ell(\ell+1)}{(i-2)} g_{i-1} \tag{87}
$$

and putting these results into equation 84, one obtains

$$f'_{i+1} = \frac{1}{2(i+1)}\left[\ell(\ell+1) - i(i-1)\right] f_i \tag{88}$$

This equation indicates that the reciprocal power series in r terminates after $i = \ell + 1$ terms for F and G, while it terminates after $i = \ell + 2$ terms for E_r.

Now, the quantity we are really interested in finding is the value of E_θ at the outer boundary of the radial mesh. From equations 73 and 74

$$E_\theta = \frac{F + G}{2} . \tag{89}$$

If we then use equations 80, 81, and 86, one obtains

$$E_\theta = \tfrac{1}{2}\left[f_0 + \frac{f_1}{r} + \frac{f_2\left(1+\frac{2}{\ell(\ell+1)}\right)}{r^2} + \cdots + \frac{f_i\left(1+\frac{i(i-1)}{\ell(\ell+1)}\right)}{r^i} + \cdots\right] \tag{90}$$

Now, from the finite difference equations for $r < R_{max}$ we can find E_θ at all mesh points except the last one (at $r = R_{max}$). The value of E_θ at the next to the last mesh point is used to match the interior problem with the outgoing wave condition. The outgoing wave expression for E_θ (equation 90) is then evaluated at $r = R_{max}$ to give the proper boundary condition. To do this we must evaluate the various f_i coefficients as a function of time.

If n_r refers to a retarded time mesh, then

$$f_i^{n_r+1} = f_i^{n_r} + \frac{\delta\tau}{2}\left[f_i'^{n_r+1} + f_i'^{n_r}\right] \tag{91}$$

where $\delta\tau$ is the size of the retarded time step. However, from equation 88,

$$f'_i = \frac{1}{2i}\left[\ell(\ell+1) - (i-1)(i-2)\right] f_{i-1} \tag{92}$$

Putting these two equations together,

$$f_i^{n_r+1} = f_i^{n_r} + \left[d_i\, f_{i-1}^{n_r+1} + f_{i-1}^{n_r}\right] \tag{93}$$

where

$$d_i = \frac{\delta\tau}{4i}\left[\ell(\ell+1) - (i-1)(i-2)\right] \tag{94}$$

Note, however, that we can now write

$$f_{i-1}^{n_r+1} = f_{i-1}^{n_r} + d_{i-1}\left[f_{i-2}^{n_r+1} + f_{i-2}^{n_r}\right] \tag{95}$$

and that $f_{i-1}^{n_r+1}$ in Equation 93 can be replaced by the expression in Equation 95. By continuing this iterative process, one can write $f_i^{n_r+1}$ in terms of $f_0^{n_r+1}$ and f_i at the previous time step; i.e.,

$$\begin{aligned} f_i^{n_r+1} = \Big\{ & f_i^{n_r} + 2d_i\, f_{i-1}^{n_r} + 2d_{i-1}\, d_i\, f_{i-2}^{n_r} + \cdots \\ & + 2d_i\, d_{i-1}\, d_{i-2} \cdots d_{i-j}\, f_{i-j-1} + \\ & d_i\, d_{i-1}\, d_{i-2} \cdots d_1\, f_0^{n_r} \Big\} + \\ & \left[d_i\, d_{i-1}\, d_{i-2} \cdots d_1\right] f_0^{n_r+1} \end{aligned} \tag{96}$$

For convenience, let

$$\left\{\ \right\} = A_i$$

$$\left[\ \right] = B_i$$

then

$$f_i^{n_r+1} = A_i + B_i\, f_0^{n_r+1} \tag{97}$$

We can now re-write Equation 90 as

$$E_\theta^{n_r+1} = \tfrac{1}{2} f_0^{n_r+1} C + D \tag{98}$$

where

$$C = 1 + \frac{B_1}{r} + \frac{B_2}{r^2}\left(1 + \frac{2 \cdot 1}{\ell(\ell+1)}\right) + \cdots + \frac{B_i\left(1 + \frac{i(i-1)}{\ell(\ell+1)}\right)}{r_i}$$

$$+ \cdots + \frac{2B_{\ell+1}}{r^{\ell+1}} \tag{99}$$

$$D = \frac{A_1}{r} + \frac{A_2}{r^2}\left(1 + \frac{2 \cdot 1}{\ell(\ell+1)}\right) + \cdots + \frac{A_i\left(1 + \frac{i(i-1)}{\ell(\ell+1)}\right)}{r^i}$$

$$+ \cdots + \frac{2A_i}{r^{\ell+1}} \tag{100}$$

The new value of f_0 is then just given by

$$f_0^{n_r+1} = \frac{2E_\theta^{n_r+1} - D}{C} \tag{101}$$

Overall, the outer boundary condition is handled in the following manner. At a given time t the fields are known at all points in the radial mesh. Difference Equations 42, 43, and 44 are then used to find the new values of the fields at time t + δt at all points except at the outer boundary. The new value of E_θ at the next to the last E_θ mesh point is then used in Equation 101 to find the new value of f_0. In doing this, one must convert from real time to retarded time (Equation 47), which is easily done at a constant r. The values of C and D in Equation 101 are known since all the f_i values were assumed known at the previous time step. New values of f_i are then calculated from Equation 96 using $f_0^{n_r+1}$ found from Equation 101.

Once all the new f_i values are known, E_θ at the outer boundary is then calculated from equation 90 where r is set equal to R_{max}. This gives all the needed values at the new time and the whole process can be iterated again. Initially, all the f_i values are set equal to zero since there is a transit time delay before any fields can arrive at the outer boundary.

The relationship between real time variables and retarded time variables is somewhat more complicated than indicated above. These relationships are shown in Figure 3 which plots radius r versus ct. On such a plot lines of constant retarded time appear as straight lines with slopes of 45° while lines of constant real time are horizontal. In our problem, we assume that E_θ is known at time t^n at all points in the radial mesh (i.e., at points 1 and 2 in Figure 3). The interior difference equations are used to find E_θ at the next to the last radial mesh point at t^{n+1} (point 3). We then need to find E_θ at the last mesh point at time t^{n+1} (point 4). By matching the known value of E_θ at 1 or 3 to an outgoing wave expression, values of the f_i terms in equation 63 are found for a constant retarded time. By simply changing r in this equation, the field at all other points along the lines of constant τ indicated in Figure 3 can be calculated. We can thus find the value of E_θ at point 4. In LFLUX, the value of E_θ at point 5 was used, so that linearly interpolating one obtains

$$E_{\theta 4} = \frac{E_{\theta 2}\ (\delta r - c\delta t) + E_{\theta 5}\ c\delta t}{\delta r} \quad . \tag{102}$$

SURFACE CURRENT AND CHARGE DENSITIES

Once the fields in space have been calculated as a function of time, it is simple to find the current density, $\vec{K}$, and charge density, σ, on the surface of the sphere from the boundary conditions at a perfect conductor; namely

$$\hat{n} \times \vec{B} = \frac{1}{\mu_0} \vec{K} \tag{103}$$

$$\hat{n} \cdot \vec{E} = \frac{\sigma}{\varepsilon_0} \tag{104}$$

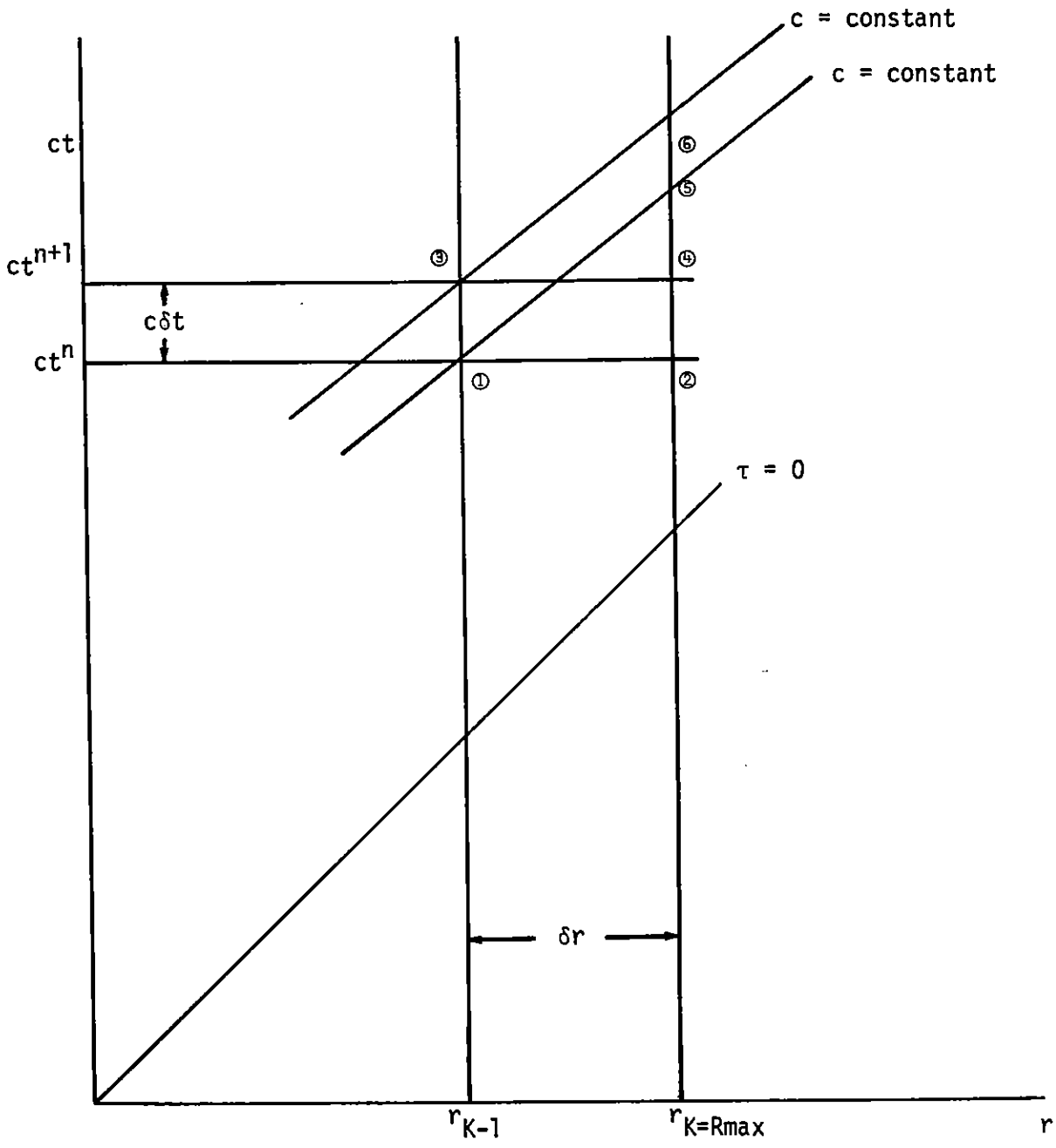

Figure 3. Illustration for interpolation from retarded to real time.

where $\hat{n}$ is a unit vector normal to the surface of the sphere and $\vec{E}$ and $\vec{B}$ are the electromagnetic fields at the surface. In this case, $\hat{r}$ is just a unit vector in the radial direction and thus

$$K_\theta = - \mu_0 B_\phi \tag{105}$$

$$\sigma = \varepsilon_0 E_r \tag{106}$$

Note that for the inner boundary condition we just assumed that E_θ was zero so that E_r and B_ϕ are the resulting fields when Maxwell's equations are solved.

TEST PROBLEM

With any reasonably complicated computer code it is good practice to devise some test problem with a known solution for use in checking both the accuracy of formulation and programming. In the case of LFLUX it was necessary to devise both a test source current and an electromagnetic problem with known solution.

Test Source Current

Thus far we have not discussed the source current term, $\vec{J}$, in Maxwell's equations. In practice, $\vec{J}$ is calculated as a function of space and time from the time history, angular distribution and energy distribution of backscattered electrons. $\vec{J}$ is then expanded in terms of Legendre polynomials and used as an input to the LFLUX code. For test purposes, however, a simplified source current was developed.

For this test current it was assumed that monoenergetic electrons are emitted in the radial direction uniformly over half the sphere. Thus, at any time t, the spatial variation of the current density is described by

$$\vec{J}\,(r,\theta) = J_0 \frac{a^2}{r^2} U\left(\frac{\pi}{2} - \theta\right)[U(v_0 t - r) - U(v_0(t-t_1) - r)]\hat{r} \tag{107}$$

where

J_0 = the current density leaving the surface of the emitting sphere (r=a) at time

U = unit step function

v_0 = electron velocity

t_1 = total emission pulse length

and $\hat{r}$ = unit radial vector.

From this expression, J_θ is zero and we need only expand J_r in Legendre polynomials; i.e.,

$$J_r = \sum_\ell J_{r_\ell} P_\ell^0 (\cos\theta) . \tag{108}$$

Thus

$$J_{r_\ell} = \frac{2\ell + 1}{2} \int_0^\pi J_r P_\ell^0 (\cos\theta) \sin\theta d\theta$$

$$= \frac{2\ell + 1}{2} J_0 \frac{a^2}{r^2} \int_0^1 P_\ell(x)dx \tag{109}$$

where we have used Equation 107 and have dropped the step functions indicating the spatial extent of the current. The integral in Equation 109 is easily evaluated for the first few values of ℓ with the result

$$J_{r_0} = \frac{1}{2} J_0 \frac{a^2}{r^2} \tag{110}$$

$$J_{r_1} = \frac{3}{4} J_0 \frac{a^2}{r^2} \tag{111}$$

$$J_{r_2} = 0 \tag{112}$$

$$J_{r_3} = -\frac{7}{16} J_0 \frac{a^2}{r^2} \tag{113}$$

$$J_{r_4} = 0 \tag{114}$$

$$J_{r_5} = \frac{11}{32} J_0 \frac{a^2}{r^2} \tag{115}$$

Using these Legendre coefficients and the step-functions of Equation 107 to determine the proper turn-on times we have expressions for $J_{r_\ell}(r,t)$ to put in the difference equations.

DELTA FUNCTION EXCITATION

The separation of variables technique has been used to analytically solve for the resulting skin currents on a perfectly conducting sphere excited by some delta function (in time) driver. (See reference 8.) After the driver has shut off, the skin currents are described by a summation of the various modes of the sphere, each mode having some characteristic oscillation frequency and decay time. These modes are tabulated in several places.

Calculation of these spherical modes depends on a Legendre polynomial expansion. However, as the order of the Legendre polynomial increases there are correspondingly more modes (corresponding to roots of the spherical Bessel function or its derivative). Thus for higher ℓ values, the results of LFLUX will correspond to the summation of several modes. For $\ell = 1$, however, there is only one resonant frequency and one decay time and these should serve as a good check between LFLUX and analytic calculations.

For this comparison the simplified source current previously discussed was used to drive a sphere of radius one meter for some short time. The driving current is then set equal to zero at all points in space for all subsequent times. The source current just serves to set up some initial distribution of skin current and charge on the surface of the sphere. After it is shut off, the skin current should just oscillate and decay in a manner determined by the resonant modes of the sphere.

Figures 4 and 5 show the results of such a calculation using LFLUX. For this calculation the driving current was shut off at 10 nanoseconds, a one meter radius sphere was assumed, and an outgoing wave outer boundary condition was used at r = 10 meters. Also, a fractional stability of f = 1.0 and a radial step of 10 cm was used.

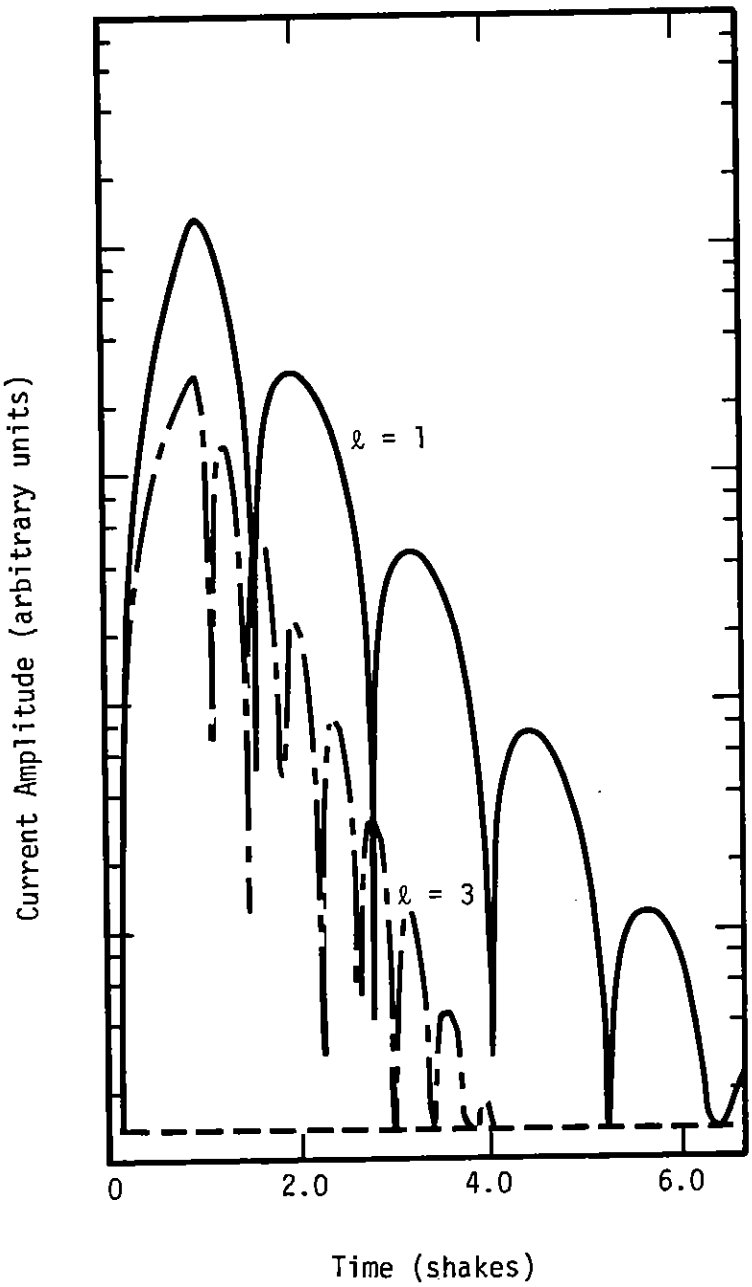

Figure 4. Amplitude of Legendre polynomial expansion of skin currents as a function of time: Test case—spatial current density shut off at t = 1.0 shake.

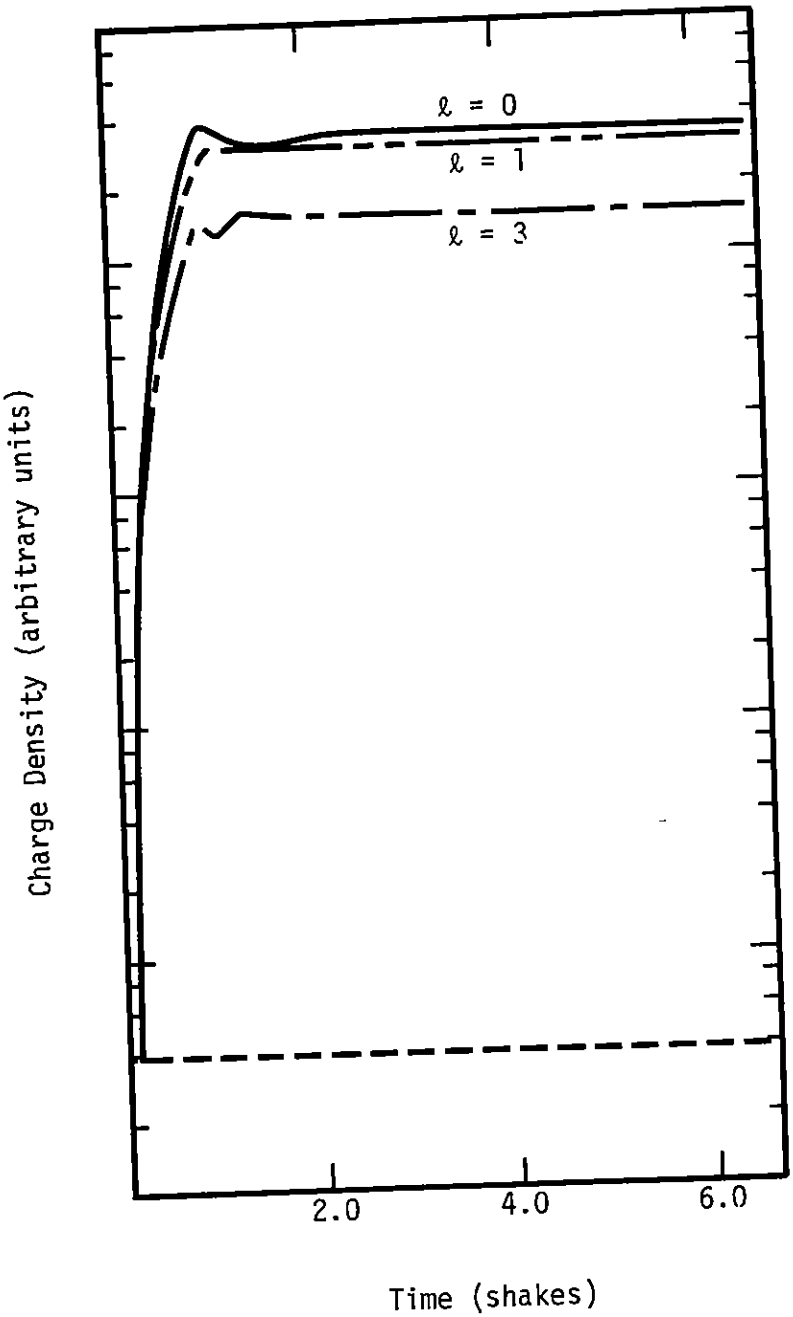

Figure 5. Amplitude of Legendre polynomial expansion of surface charge densities as a function of time: Test case—spatial current density shut off at t = 1.0 shakes.

Figure 4 shows plots of the $\ell = 1$ and $\ell = 3$ Legendre coefficients of the skin current as a function of time. A number of important features of of these plots should be noted. First of all, the curves are obviously very nearly damped sinusoids for times greater than 10 nanoseconds (when the source current is shut off everywhere). Note that the curves actually plot the absolute value of the skin current on a logarithmic scale. The frequency and decay time of the $\ell = 1$ curve in this time interval can be measured from the plot as

$$\text{measured frequency} = \omega_{\ell=1} = 2.58 \times 10^{8} \text{ sec}^{-1} \tag{116}$$

$$\text{measured decay time} = \tau_{\ell=1} = 6.82 \times 10^{-9} \text{ sec} \tag{117}$$

In this case it has been assumed that the skin current is described by the equation

$$K = K_o \, e^{i\omega t} \, e^{-\frac{t}{\tau}} \tag{118}$$

For the lowest frequency mode, ω and τ are analytically calculated to be

$$\omega_{\ell=1} \simeq \frac{.86c}{a} \simeq 2.58 \times 10^{8} \text{ sec}^{-1} \tag{119}$$

$$\tau_{\ell=1} \simeq \left(\frac{.5c}{c}\right)^{-1} \simeq 6.66 \times 10^{-9} \text{ sec} \tag{120}$$

It is readily seen that we have good agreement between the numerical and analytic values.

The $\ell = 3$ curve is actually a combination of two modes (see Reference 8) but one of these modes damps much faster than the other so that the resultant curve just closely resembles a damped sinusoid with the slower decay time.

Figure 5 is a plot of the Legendre polynomial expansion coefficients of the surface charge density as a function of time. One can use these curves and those in the previous figure to show that the surface continuity equation (equation 1) is satisfied.

Rather than the various Legendre polynomial coefficients, one is usually interested in the currents or charge densities at some angle θ with respect to the axis of the sphere. To find these values one uses equations 105 and 106. In the case of LFLUX, K_ℓ and σ_ℓ are calculated for only the first few values of ℓ. It is readily seen that the values of K_ℓ and σ_ℓ decrease as ℓ increases (except at very early times). Thus, the fact that the series contains only the first few ℓ values is not very important (i.e., the series converges very rapidly).

Because of the expansion in Legendre polynomials, LFLUX is limited to spherical geometries. A typical LFLUX run requires 15-20 sec of time on the CDC 7600.

SECTION 4

RESULTS

In this section results will be presented which show the importance of X-ray time history on skin currents. Comparisons between two methods of calculating skin currents will also be made in this section. The X-ray pulse is described by the time function $\sin^2(\pi t/T)$ where the pulse ends when $t = T$, and where T is defined as the pulse length. The emitted electrons that form the spatial current are the result of a black body X-ray spectrum interacting with an aluminum sphere 1 meter in radius. Electrons are ejected from the sphere with a $\cos\theta$ distribution. Figures 6 through 8 show a comparison of FIELD and LFLUX for the first three Legendre coefficients of the skin current for $T = 3\times10^{-8}$ sec. (In Figures 6 through 14, a thin black line represents the quasi-static calculation, when the two calculations differ.)

For each Legendre polynomial there is usually associated one dominant natural mode of the sphere although for Legendre polynomials larger than order 2 there is more than 1 natural mode. The periods of these modes decrease with the order of the polynomial. The effect of stimulating these modes can only be described by the full Maxwell time dependent equations. Differences between FIELD and LFLUX will be increasingly evident the more the natural modes are excited. The first mode of a sphere with a 1 meter radius has a period of 2.4×10^{-8} sec, the second a period of 1.2×10^{-8} sec, the third mode a period of $.8\times10^{-8}$ sec. Since the pulse length of 3×10^{-8} sec is close to the first mode of the sphere we should expect to see the greatest difference between the two codes in the skin current coefficient associated with the first Legendre polynomial coefficients.

Figures 6 through 8 show about a 20 percent difference in peak current for the first Legendre coefficient of the skin current and almost no difference for the second and third coefficients. Figures 9 through 11 show the same comparisons for $T = 1 \times 10^{-8}$ sec. Here the differences are greater, even for the second Legendre current coefficient. Table 1 (page 14) gives a quantitative idea of the correction the full time-dependent Maxwell equation solution makes upon the quasi-static solution. The calculated correction is described in the end of Section 2 and is based on viewing the difference between the two methods of solution as arising from modal excitation. The differences appearing in Figures 6 through 11 agree quite well, qualitatively, with the calculations. Figures 6 through 11 indicate that time dependent electromagnetic effects are apparent for a sphere when the lowest mode of the interacting system is about 2/3 of the X-ray pulse length.

In Figures 6 through 11 the electron energy spectrum contained electrons with energies ranging from 5 to 100 kev. If E denotes energy, these electrons have an energy distribution with the functional form $e^{-.1E}$. Cutting off the electrons whose energies range from 5 to 50 kev yields a spectrum where the electrons have an average velocity about three times higher than the average velocity of the electrons whose energies ranged from 5 to 100 kev. Figures 12 through 14 compare the two methods of finding the skin current for this high energy spectrum (with $T = 3 \times 10^{-8}$ sec). By comparing these latter figures to Figures 9 through 11 it appears, if one is concerned with currents above 1/10 of the peak value, that X-ray time history may be a more important variable, where time dependent electromagnetic effects are concerned, than average electron velocity. These results are dependent on the radius of the system, the form of the electron distribution and the pulse lengths considered.

The magnitude and time dependence of skin current depends upon the magnitude and time dependence of the spatial currents at the points external to the sphere. No matter what the velocity of the electrons they will

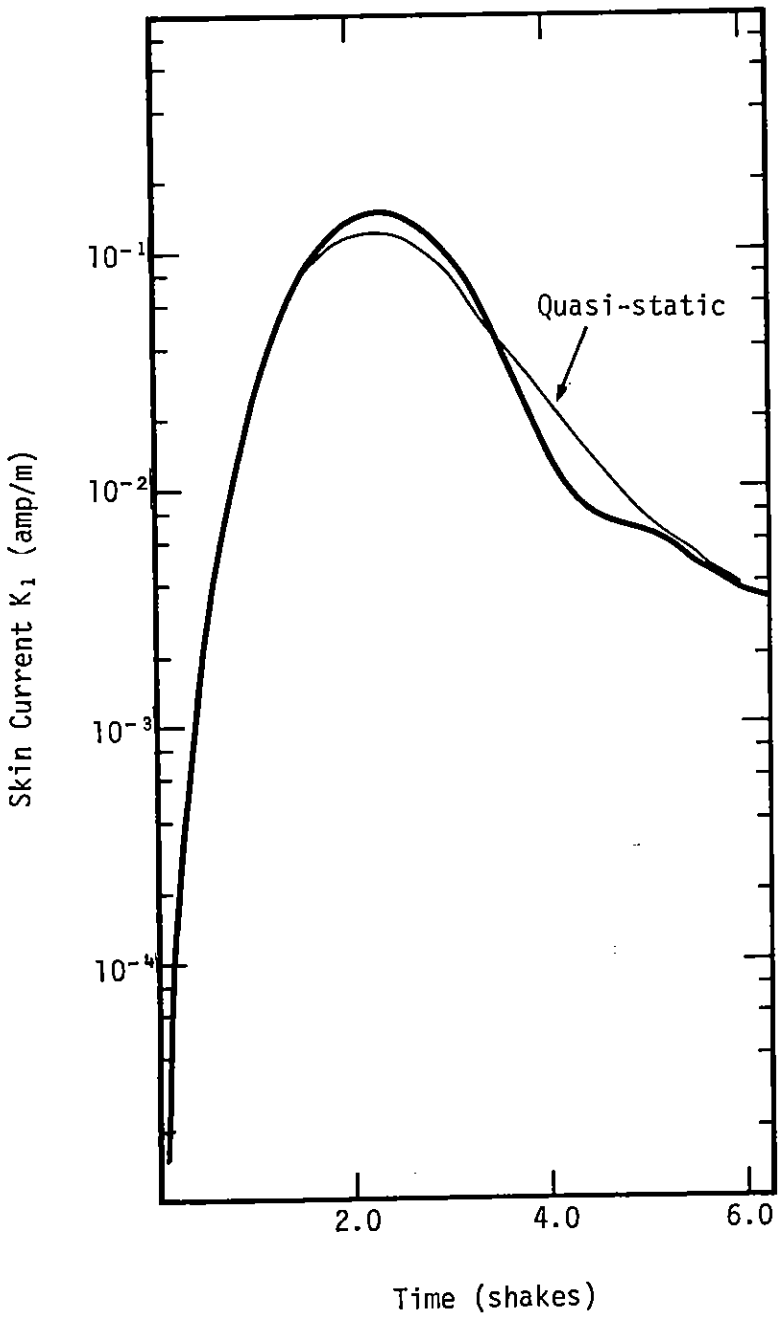

Figure 6. Comparison of $\ell=1$ skin current amplitudes.
Energy range of X rays: 5 - 100 keV.
Pulse duration: 3.0 shakes.

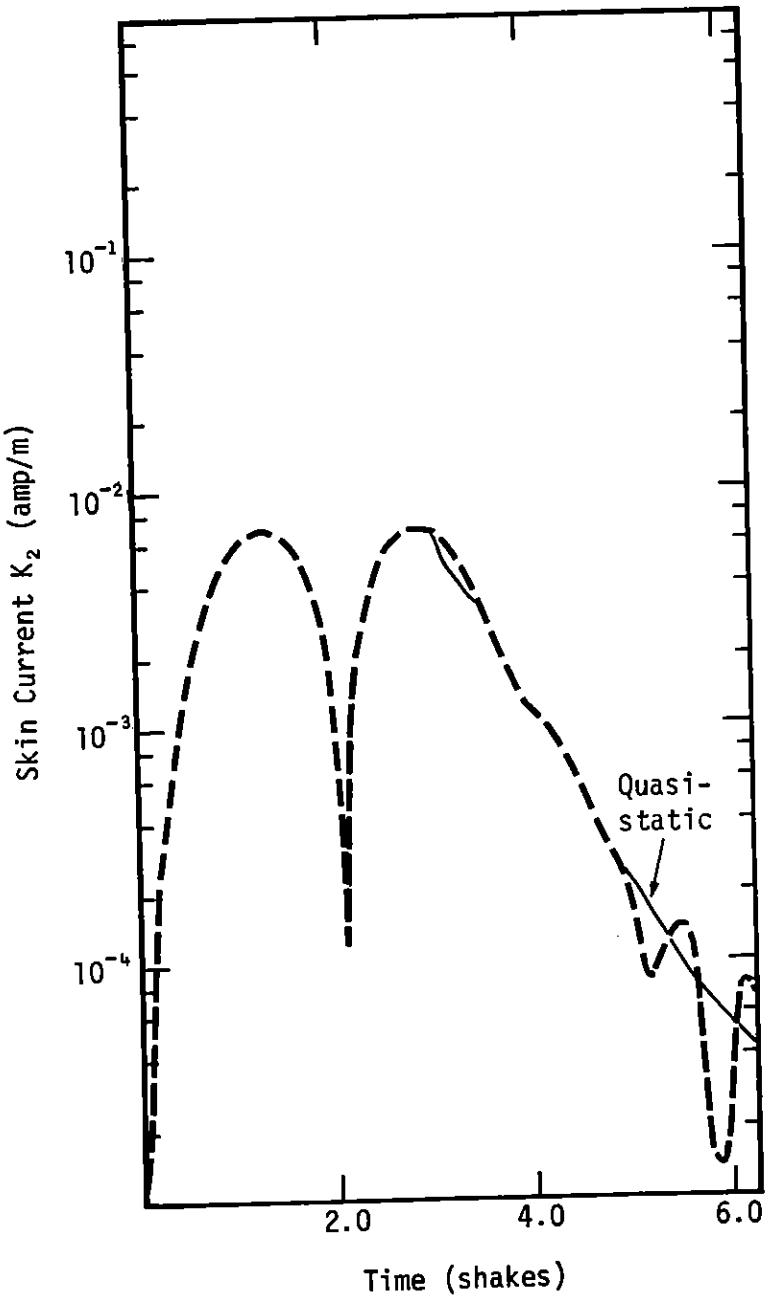

Figure 7. Comparison of $\ell=2$ skin current amplitudes.
Energy range of X rays: 5-100 keV
Pulse duration: 3.0 shakes

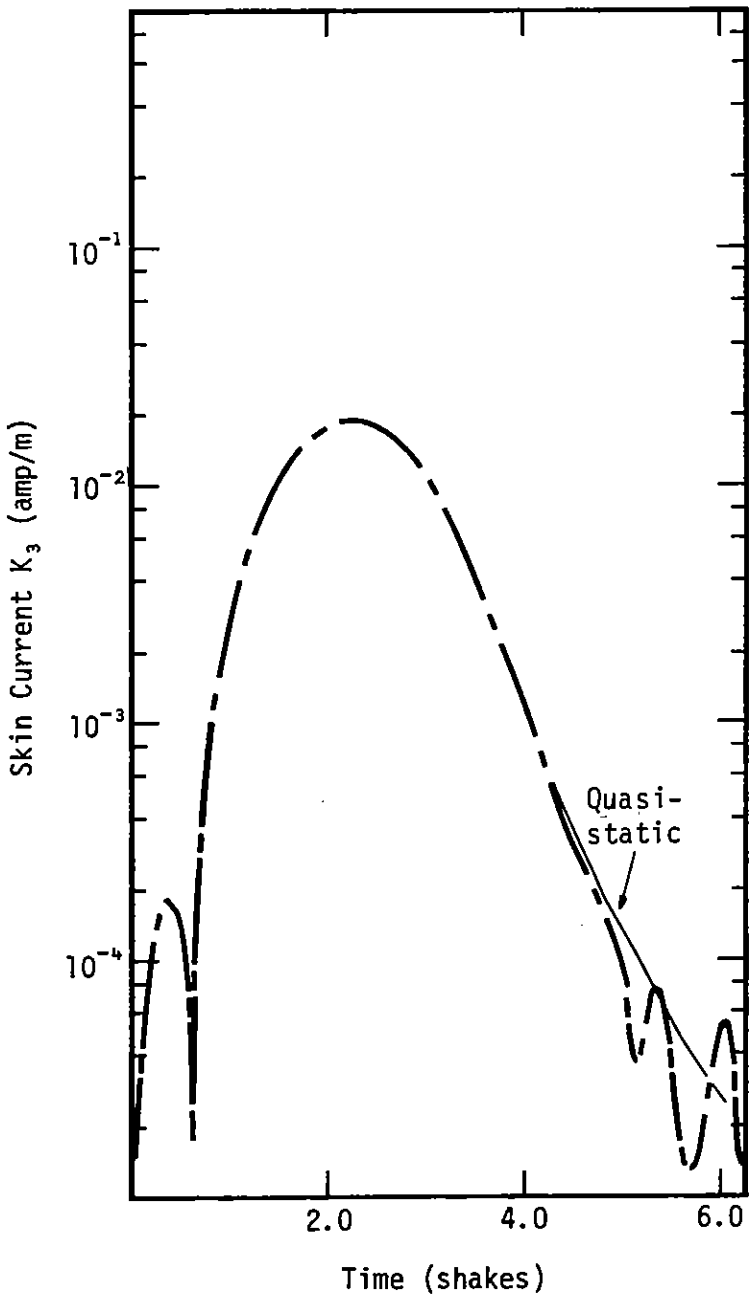

Figure 8. Comparison of ℓ=3 skin current amplitudes.
Energy range of X rays: 5-100 keV
Pulse duration: 3.0 shakes

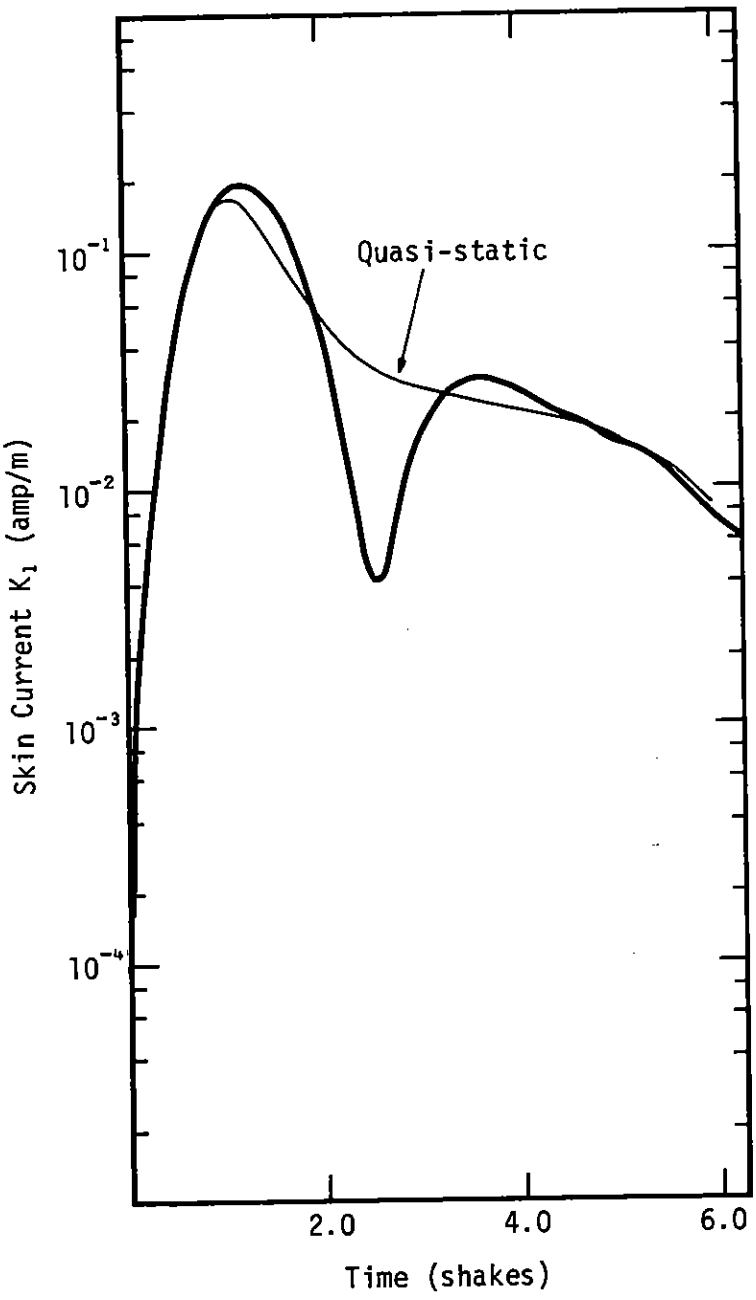

Figure 9. Comparison of ℓ=1 skin current amplitudes.
Energy range of X rays: 5-100 keV
Pulse duration: 1.0 shakes

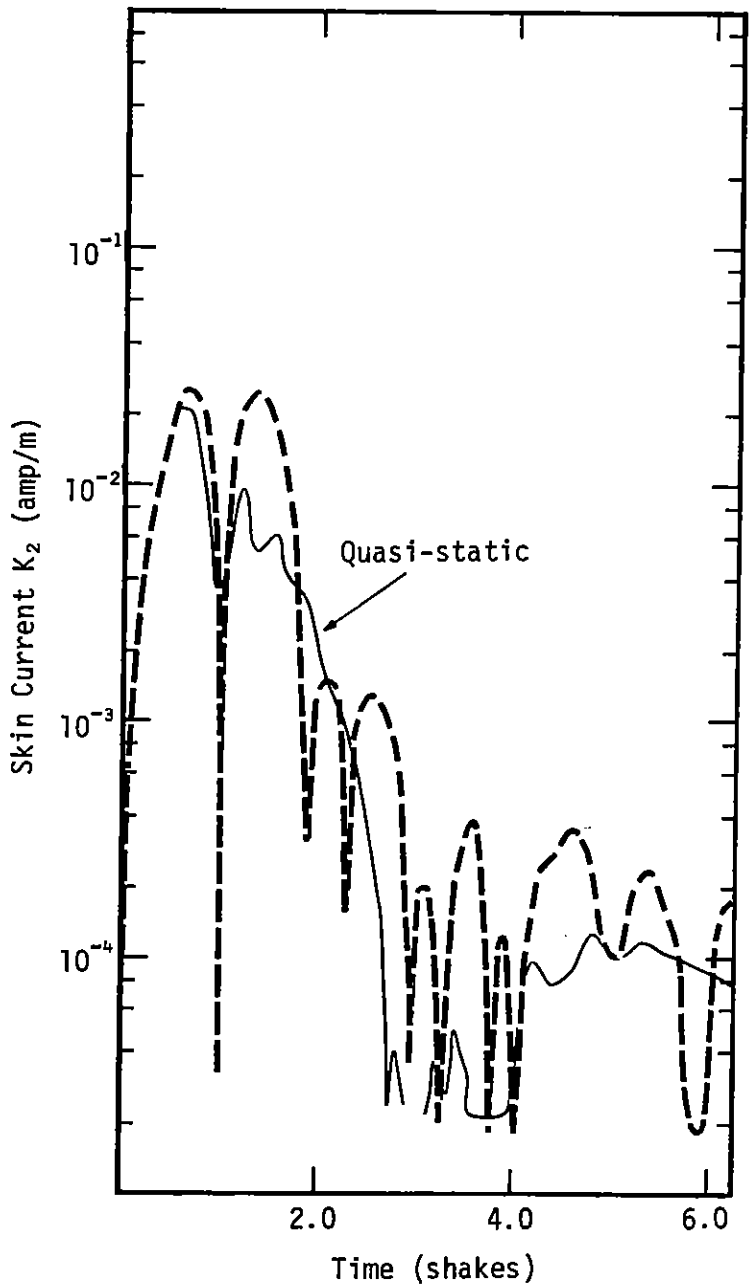

Figure 10. Comparison of ℓ=2 skin current amplitudes.
Energy range of X rays: 5-100 keV
Pulse duration: 1.0 shakes

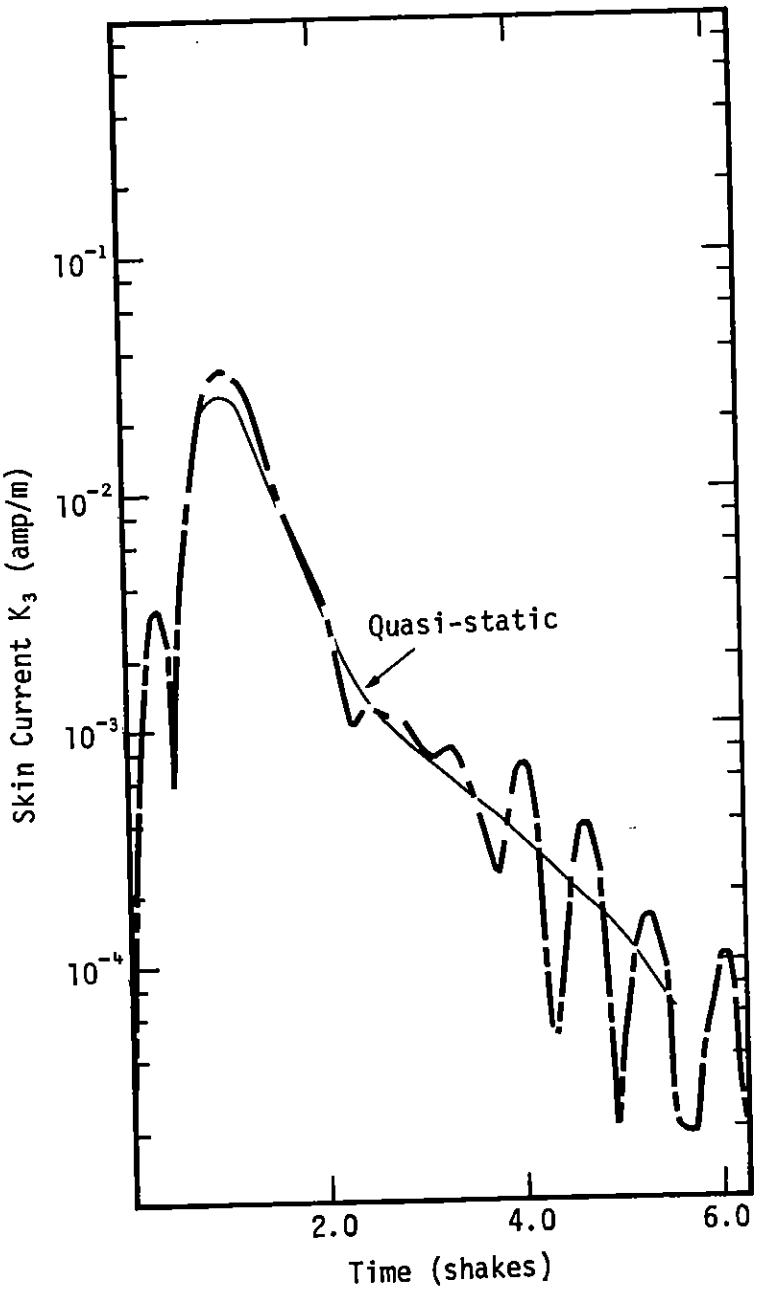

Figure 11. Comparison of ℓ=3 skin current amplitudes.
Energy range of X rays: 5-100 keV
Pulse duration: 1.0 shakes

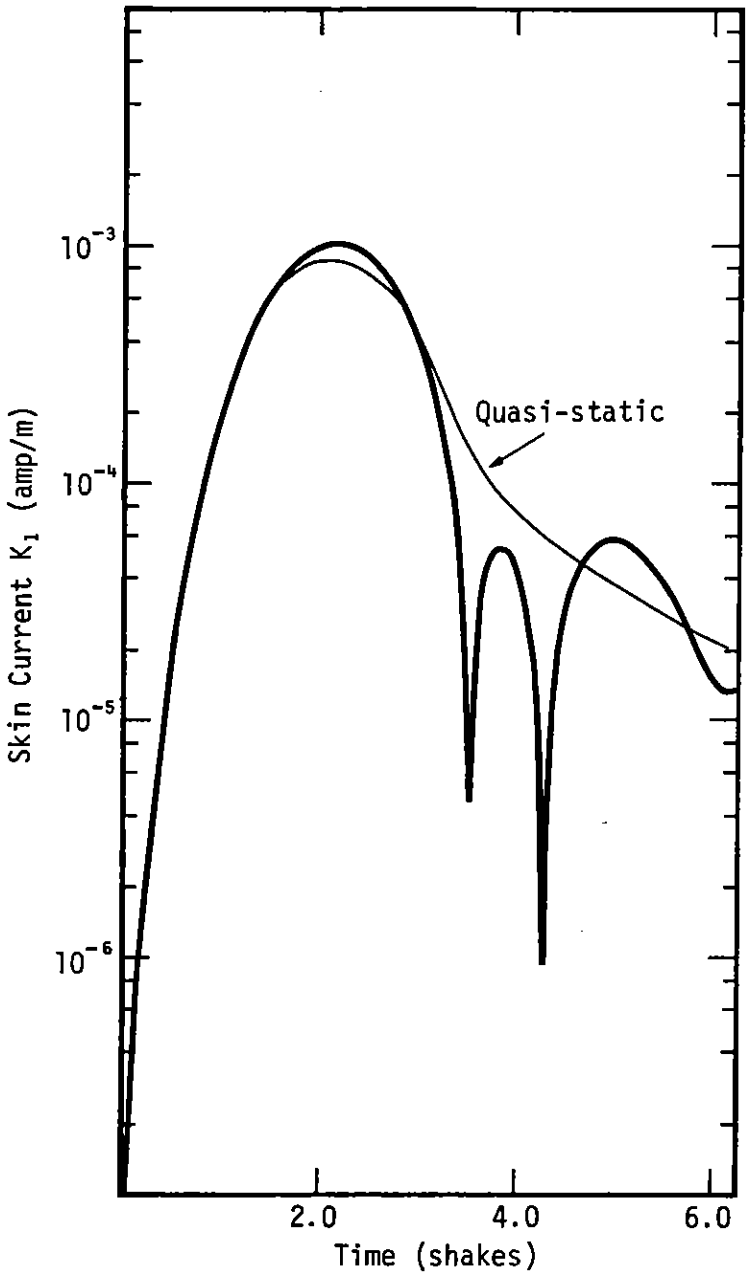

Figure 12. Comparison of ℓ=1 skin current amplitudes.
Energy range of X rays: 50-100 keV
Pulse duration: 3.0 shakes

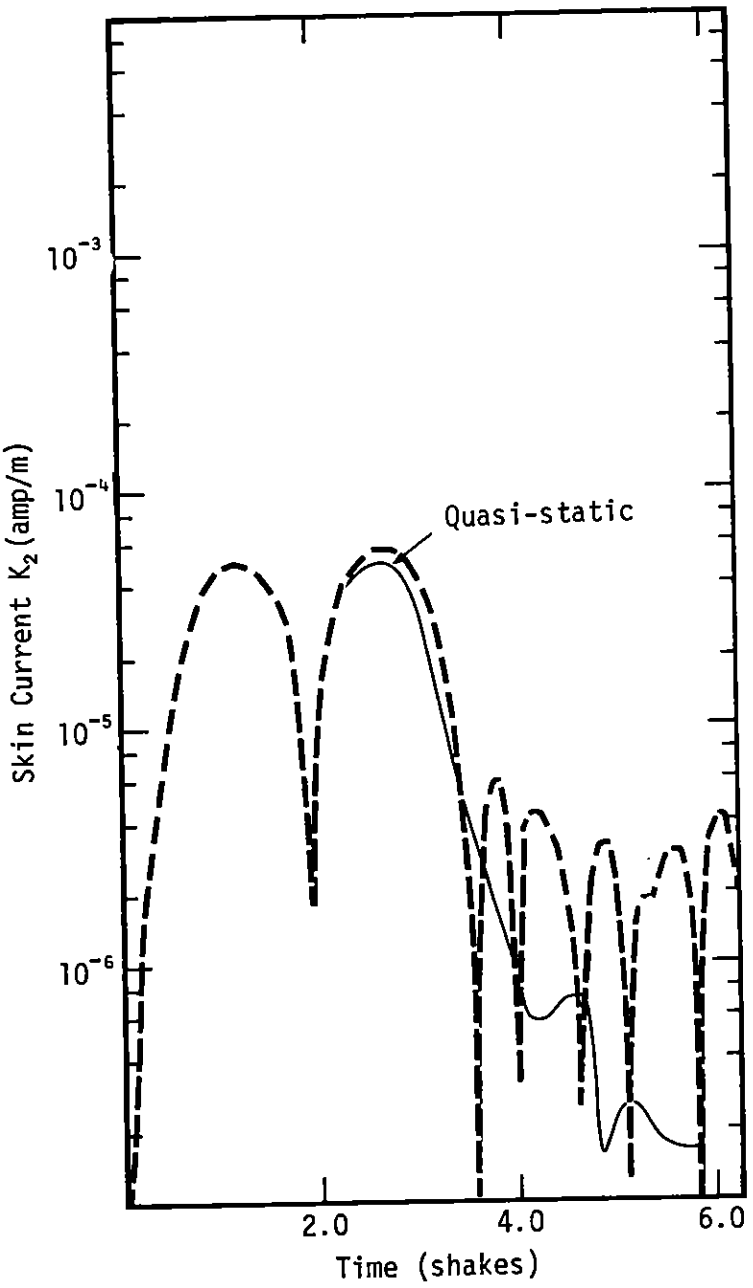

Figure 13. Comparison of $\ell=2$ skin current amplitudes.
Energy range of X rays: 50-100 keV
Pulse duration: 3.0 shakes

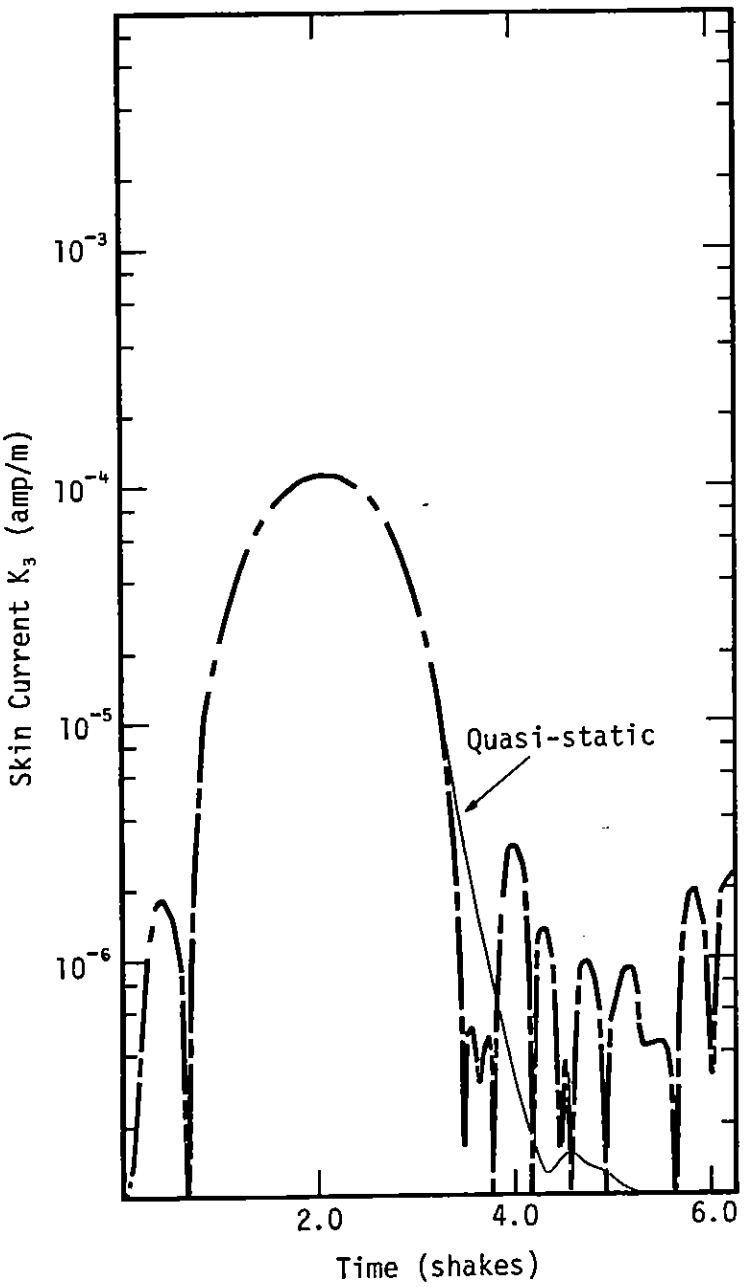

Figure 14. Comparison of $\ell=3$ skin current amplitudes.
Energy range of X rays: 50-100 keV
Pulse duration: 3.0 shakes

continue to be emitted for a time T, since the X rays interact for a time T. Thus, after the electrons first arrive at a spatial point they will continue to arrive, in the non-self-consistent limit, for a time T (in general they will arrive at a spatial point for a time greater than T, since it takes time for the electrons to get to a spatial point, see Reference 2). It is clear then that the time history of the spatial currents is very directly related to the time history of the X-ray pulse. The importance of the X-ray time history in determining skin currents, is therefore evident in a low fluence limit.

REFERENCES

1. Higgins, D. F., "X-ray Induced Photoelectric Currents," Air Force Weapons Laboratory, AFWL Theoretical Note 178, June 1973.

2. Stettner, R., "Low Fluence Calculation of Photoelectron Flux Densities Outside an Emitting Sphere," Mission Research Corporation, MRC-N-110, DNA 3411T, January 1974.

3. Jackson, J. D., Classical Electrodynamics, John Wiley & Sons, Inc., New York, 1962, p. 78.

4. Conte, S. D., Elementary Numerical Analysis, McGraw Hill, 1965.

5. Graham, W. R., "The Electromagnetic Fields Produced by a General Current Distribution in a Conductive Environment Under Certain Symmetry Considerations," Air Force Weapons Laboratory, AFWL Theoretical Note 21, January 1965.

6. Longmire, C. L., "Outer Boundary Condition for Surface Burst EMP Codes," Air Force Weapons Laboratory, AFWL Theoretical Note 70, December 1969.

7. Longley, H. J., and C. L. Longmire, "Development and Testing of LEMP 1," Air Force Weapons Laboratory, AFWL Interaction Note 75, April 1970.

8. Stratton, J. A., Electromagnetic Theory, McGraw-Hill, New York, 1941, p. 558.